

See discussions, stats, and author profiles for this publication at: <https://www.researchgate.net/publication/384110816>

Valorization of hawthorn seed waste through solid phase extraction of antibiotics from water samples

Article in *Emergent Materials* · September 2024

DOI: 10.1007/s42247-024-00865-0

CITATION

1

READS

120

7 authors, including:



Aziza Snoussi

Tunis El Manar University

2 PUBLICATIONS 6 CITATIONS

SEE PROFILE



Imen Abidli

Tunis El Manar University

7 PUBLICATIONS 12 CITATIONS

SEE PROFILE



Rafika Ben Sghaier

Tunis El Manar University

18 PUBLICATIONS 226 CITATIONS

SEE PROFILE



Latifa Latrous El Atrache

Tunis El Manar University

47 PUBLICATIONS 447 CITATIONS

SEE PROFILE



Valorization of hawthorn seed waste through solid phase extraction of antibiotics from water samples

Aziza Snoussi¹ · Imen Abidli¹ · Rafika Ben Sghaier^{1,2} · Magalie Claeys³ · Latifa Latrous^{1,4} · Adel Megrache¹

Received: 2 July 2024 / Accepted: 6 September 2024
© Qatar University and Springer Nature Switzerland AG 2024

Abstract

Removing pollutants from contaminated water is crucial for maintaining a disease-free and healthy society. The potential of a novel, cost-effective hydrochar was explored for extracting antibiotics from aqueous environments. The study employed both experimental and theoretical approaches. Agricultural waste, specifically hawthorn seeds hydrochar was prepared via hydrothermal carbonization and was characterized using IR and SEM–EDX analyses. Solid-phase extraction (SPE) of metronidazole and levofloxacin was investigated, followed by their determination using high-performance liquid chromatography (HPLC). An experimental design optimized the SPE process, focusing on sample volume, elution volume, and type of elution solvent to enhance antibiotic extraction efficiency. The optimal conditions of SPE extraction included 50 mL of sample solution, and 5 mL of methanol as the elution solvent type. The best separation was achieved with isocratic elution utilizing a mobile phase consisting of acetonitrile–water (pH = 4) with 0.4% triethylamine 25:75 (V/V). The identification of antibiotics was carried out using diode array detection, with calculations performed for the linear range, the limit of detection (LOD), and the limit of quantification (LOQ). The LOD and LOQ ranged from 0.13 to 0.2 $\mu\text{g}\cdot\text{L}^{-1}$ and from 0.62 to 0.87 $\mu\text{g}\cdot\text{L}^{-1}$, respectively. Using actual water samples, researchers evaluated the effectiveness of the optimized solid-phase extraction (SPE) method. The recoveries were exceeded 96%, with a relative standard deviation (RSD) below 9.5%, demonstrating the minimal interference from the sample matrix and confirming the robustness of the method. Additionally, a computational study for the investigation of the sorption mechanism, interaction energies, and distances between the adsorbent and adsorbate was done.

Keywords Solid phase extraction (SPE) · Mixed matrix design experimental · Hawthorn seeds hydrochar · Antibiotics · HPLC–UV · Surface water · DFT calculation

1 Introduction

The critical need for clean water necessitates the continuous development and evaluation of novel adsorbent materials for water treatment. Solid-phase extraction (SPE) stands out for its operational simplicity, making it a desirable method. However, a key challenge lies in identifying new, highly adsorbent materials. Additionally, a single material often proves insufficient for tackling the diverse range of pollutants found in water. Here, the concept of converting waste materials into adsorbents presents a promising solution. This approach not only addresses the substantial waste generation problem [1] but also offers a cost-effective path forward for water treatment technology.

Over the last two decades, in response to the environmental needs of agricultural waste disposal, emerging industries, such as hydrochar production, have been developed [2, 3] Hydrochar has attracted considerable interest due to

✉ Latifa Latrous
latifa.latrous@ipeiem.utm.tn

¹ Laboratoire de Chimie Minérale Appliquée (LR19ES02),
Faculté Des Sciences de Tunis, Université de Tunis El
Manar, Campus Universitaire El Manar I, 2092 Tunis,
Tunisie

² Laboratory of Composite Materials and Clay Minerals,
National Center of Researches in Material Sciences,
Technopole Borj Cédria, Soliman, Tunisia

³ Institut Méditerranéen de Biodiversité Et d'Ecologie Marine
Et Continentale Aix-Marseille Université - UMR CNRS IRD
Avignon Université - Site de L'Etoile - Avenue Escadrille
Normandie Niemen, 13013 Marseille, France

⁴ Institut Préparatoire Aux Etudes d'Ingénieurs d'El Manar,
B.P.244 El Manar II - 2092, Tunis, Tunisie

its sorption processes. The sorption capacity of hydrochar depends on the surface forces' ability to attract compounds from various media. The adsorption process involves a combination of strong forces like electrostatic attraction and weaker forces like van der Waals forces, stacking interactions, and hydrogen bonding [4–6].

Hydrochar produced from agro-industrial waste has been investigated. Date stone-derived hydrochar was employed in the microextraction of nonsteroidal anti-inflammatory drugs from aqueous samples [7, 8].

Solid-phase extraction (SPE) has become a well-established technique for selectively separating and concentrating diverse pollutants from environmental samples, even when those pollutants are present at trace levels. It involves selectively adsorbing analytes onto a solid phase and then eluting them with a solvent, thereby isolating and concentrating the analytes from complex matrices for further analysis. The most challenging and time-consuming aspects of solid phase extraction is optimizing the various factors that influence the extraction process. However, the traditional approach of optimizing each factor individually (one-at-a-time) can be misleading, particularly when interactions exist between these factors. Experimental designs enable the simultaneous optimization of multiple variables, which can be both qualitative and quantitative. This is why mixed designs are valuable. They provide mathematical models to assess the relevance and statistical significance of each factor's effect on the process, as well as the interactions among the factors [9].

Green water treatment technologies rely not only on maximizing the performance of adsorbent materials but also on a deep understanding of how these materials capture pollutants. Biochars, a promising class of green adsorbents, possess active sites rich in oxygen, sulfur, and nitrogen, which are believed to play a crucial role in pollutant adsorption. The focus on solely increasing adsorption capacity in biochars might hinder a complete understanding of the removal mechanisms. Investigating adsorbent-adsorbate interactions is crucial for optimizing these green technologies [10]. The concepts of DFT are useful for analyzing both molecules involved in reactions and isolated molecules [11, 12]. Modeling of the phenomenon of adsorption using the DFT technique establishes a significant correlation between specific microscopic parameters and experimentally measurable macroscopic quantities [13, 14].

Intending to improve water treatment methods, this work explores the impact of functional groups on hydrochar surfaces for the adsorption of antibiotics (ATB) present in environmental water samples. This widespread presence of antibiotics in water bodies has raised significant concerns due to their detrimental impacts on aquatic ecosystems [15]. Numerous studies have documented the adverse effects of antibiotic-laden wastewater on aquatic life, including fish

populations in rivers [16]. Moreover, artificial water reservoirs are particularly vulnerable to the ecological risks posed by most antibiotics, with algae and invertebrates being especially susceptible. The contamination of various water environments not only endangers aquatic organisms but also presents a substantial threat to human health, especially when exposed to antibiotic mixtures [17].

Given the FDA's concern about aquatic environments containing pharmaceutical compounds exceeding 1 µg/L [18], Hawthorn biochar was synthesized and characterized. Hawthorn is commonly found growing and popular in Tunisia. The obtained adsorbent was used from water samples for solid-phase extraction of Levofloxacin (LEVO) and Metronidazole (MNZ) antibiotics.

The utilization of a mixed factorial design, incorporating both quantitative and qualitative parameters, has been emphasized [19]. The factorial experimental design was conducted to examine the impact of sample volume (V_s), solvent elution volume (E_v), and nature of solvent elution (S_n) on extraction recovery. Determination of antibiotics was carried out by liquid chromatography coupled to UV–Vis detection. Following optimization, the method's efficacy was rigorously validated and demonstrated by the successful application to real surface water samples. Preliminary insights into the chemical interactions governing antibiotic adsorption onto hydrochar surfaces were gained by calculating electronic parameters, including the energy of the highest occupied molecular orbital (EHOMO), the energy of the lowest unoccupied molecular orbital (ELUMO), the Fukui index, and the electrostatic potential (ESP).

2 Materials and methods

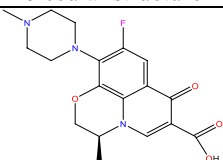
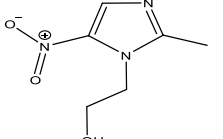
2.1 Chemicals and standard solutions

Levofloxacin (LEVO) and Metronidazole (MNZ) were purchased from Sigma-Aldrich (Saint-Louis, USA) with a purity of 98%. Water, acetonitrile (CAN) and methanol (MeOH) are all of HPLC grade and purchased from Fisher Chemical. Triethylamine (TEA) was supplied from FLUKA. Orthophosphoric acid, sodium acetate, acetic acid, and potassium dihydrogen phosphate were purchased from Sigma-Aldrich (Saint-Louis, USA). The chemical structures of selected compounds are shown in Table 1. A stock solution of LEVO and MNZ was prepared at 1000 µg L⁻¹ concentration and stored at 4°C. Working solutions were diluted at various concentrations of the prepared standard solutions.

2.2 Hawthorn seeds hydrochar synthesis (HSHC)

The hawthorns were produced in northern Tunisia. Hawthorns were collected from ESSAREJ mountain in Siliana

Table 1 Molecular structure and main physicochemical properties of the studied antibiotics

Antibiotics	Molecular structure	Brut formula	pKa
Levofloxacin		C ₁₈ H ₂₀ FN ₃ O ₄	6.25
Metronidazole		C ₆ H ₉ N ₃ O ₃	2.57 15.42

city. After being washed with deionized water and dried in the oven at 50°C for three days to eliminate all impurities, the hawthorn seeds were crushed and sieved into particles < 60 mesh. Then, 1.5 g of seeds were mixed with 9 ml of deionized water and 5g of ZnCl₂. The mixture was stirred for 10 min and included into 20-mL a Teflon autoclave at 200°C for 10 h. Finally, the obtained hydrochar was rinsed with distilled water and dried at 80°C overnight. The process is shown in Fig. 1.

2.3 Characterization of HSHC

The characterization of HSHC was performed using a Fourier transform infrared (FT-IR) in the mid-infrared region (400–4000 cm⁻¹) to identify the surface functional groups and scanning electron microscopy (SEM) to investigate its elemental composition. The mineralogical composition of HSHC was analyzed by X-ray diffraction analysis (XRD) using an (X'Pert PRO MPD) between 0.5° and 80° in the 2θ range.

The point of zero charge (PZC) of HSHC was determined using the pH drift method. This involved adjusting the pH of solutions ranging from 2 to 10 using NaOH and HCl solutions. Subsequently, 0.2 g of HSHC was added to 10 mL of each pH-adjusted solution and stirred for 24 h [7].

To determine the PZC, the initial pH of each solution (pH_i) and the final supernatant pH (pH_f) after 24 h of stirring were plotted on a graph. The pH_{PZC} was identified as the pH

value at which the curve representing pH_i vs. pH_f intersects with the line where pH_i = pH_f.

2.4 Instruments and operating conditions

The chromatographic analyses were performed using an HPLC system with a quaternary pump (SYKAM S 1125, Germany) and UV–Vis detector (SYKAM S3245, Germany). The column was a Thermo Electron Corporation C18 (250 mm × 4.6 mm D.I, dp = 5 μm). Advanced chromatography software (Clarity, DataApex Czech Republic) was used for data management and setting up the analyses. HPLC separation of the antibiotics was completed in 3 min less than 5 min under isocratic elution of 0.1% TEA solution (pH = 4) and ACN (75: 25, v/v), the pH was adjusted with orthophosphoric acid (85%) and its flow rate was set to 1.0 mL min⁻¹. The detection wavelength of the detector was set to 310 nm and the injected volume was 20 μL.

2.5 Batch adsorption experiments

To verify the adsorption of the studied antibiotics on the synthesized HSHC, 10 mg of HSHC was added to 10 mL of purified water spiked with 1 mL of LEVO and MNZ solution with a concentration of 10 mg/L. The mixture was stirred in an ultrasound unit under various experimental conditions. The contact time ranged from 0 to 70 min, at

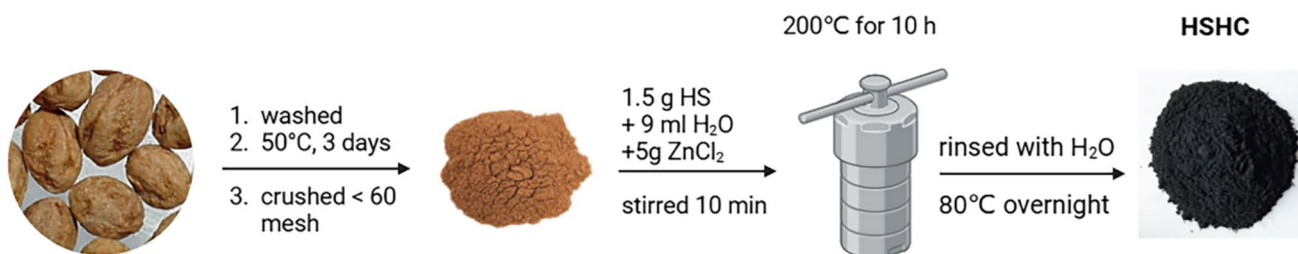
**Fig. 1** Preparation of activated carbon from hawthorn seed waste

Table 2 Kinetic and equilibrium models equations [20]

	Equations	Parameters
	$Q(\text{mg g}^{-1}) = (C_0 - C_e) \frac{V}{W} \quad (1)$	C_e (mg L^{-1}) equilibrium concentration, C_0 (mg L^{-1}) initial concentration, V (mL) volume and W (mg) mass
	$\% \text{ Adsorption} = \frac{C_0 - C_e}{C_0} \times 100 \quad (2)$	C_0 (mg L^{-1}) initial concentration, C_e (mg L^{-1}) equilibrium concentration
Kinetic models		
Pseudo-first order	$\ln(q_e - q_t) = \ln q_e - (k_1 t) \quad (3)$	k_1 (min^{-1}) constant rate of pseudo-first order; q_e (mg. g^{-1}) and q_t (mg. g^{-1}) are the adsorption capacities of the adsorbent at equilibrium
Pseudo-second order	$\frac{t}{qt} = \frac{1}{(k_1 \times q_e^2)} + \frac{1}{q_t} \quad (4)$	k_2 ($\text{g mg}^{-1} \text{min}^{-1}$) constant rate of pseudo-second order; q_e (mg g^{-1}) theoretical value of the adsorption capacity
Isotherm models		
Langmuir	$q_e = \frac{q_m k_L C_e}{1 + k_L C_e} \quad (5)$	q_m (mg g^{-1}) maximum adsorption capacity; K_L (L mg^{-1}) Langmuir constant; C_e (mg L^{-1}) equilibrium concentration
Freundlich	$q_e = K_F C_e^{1/n} \quad (6)$	K_F (mg g^{-1}) (mg L^{-1}) $^{-1/n}$; $1/n$ Freundlich constant; C_e (mg L^{-1}) equilibrium concentration

pH = 4, and at ambient temperature levels. The mathematical models used in this study are summarized in Table 2.

2.6 SPE experiments

Agilent SampliQ C18 cartridges (0.2 g, 3 mL, polypropylene) were modified to create HSHC-packed cartridges. First, the C18 stationary phase was removed from the cartridge using a vacuum. Subsequently, 50 mg of HSHC was packed into the emptied cartridge. Polypropylene frits were placed at both ends to prevent the HSHC from moving and secure it within the cartridge. The prepared cartridge was then placed in a vacuum elution apparatus. Prior to sample application, the HSHC cartridge was activated by passing 5 mL of methanol followed by 5 mL of deionized water through it. Next, a known volume of sample water containing the two target antibiotics was loaded onto the cartridge. The retained antibiotics were then eluted with an optimized volume of organic solvent. Finally, the eluted extract was concentrated using a Kuderna-Danish apparatus with a stream of nitrogen to a final volume of 1 mL. Recovery was determined using the following equation:

$$R\% = \frac{C_0 - C_e}{C_0} \times 100 \quad (7)$$

where C_0 (mg L^{-1}) initial concentration, C_e (mg L^{-1}) equilibrium concentration.

2.7 Experimental design

In this work, a mixed experimental design is used to determine the optimum conditions for the solid-phase extraction of antibiotics from an aqueous solution with a minimum number of experiments. To examine the effect of parameters on the recovery efficiency (%) of antibiotics, sample volume (U_1), solvent elution volume (U_2), and nature of solvent elution (U_3) were taken as independent variables, each factor having two levels as seen in Table 3.

Eighteen ($N = 18$) experiments were conducted to investigate the key factors affecting the recovery efficiency of antibiotics using HSHC cartridge in SPE extraction and any potential interactions between these factors. To account for potential errors, the experiment at the center point (representing average factor levels) was repeated three times. Additionally, the order of experiments was randomized to minimize any systematic bias in the evaluation.

The measured response (Y) for each experiment was the antibiotic recovery efficiency ($R\%$) achieved with the HSHC cartridge. A second-order model was then developed to describe the relationship between the factors and the recovery efficiency. This model allows us to predict the recovery efficiency across the entire range of investigated factor combinations using the following Eq. (8):

Table 3 Experimental domain

	Name	Short name	Unit	Central value	Variation range
Factor 1	Sample volume	V_s	mL	100	50
Factor 2	Elution volume	E_v	mL	3	2
Factor 3	Nature of solvent elution	S_n			

$$\begin{aligned}
 Y = & b_0 + b_1X_1 + b_2X_2 + b_{3A}X_3 + b_{3B}X_3 \\
 & + b_{11}X_1^2 + b_{22}X_2^2 + b_{12}X_1X_2 + b_{13A}X_1X_{3A} \\
 & + b_{13B}X_1X_{3B} + b_{23A}X_2X_{3A} + b_{23B}X_2X_{3B}
 \end{aligned} \quad (8)$$

where b_i characterizes the estimation of the principal independent effects of factor i , b_{ii} is the estimation of the second-order effects, and b_{ij} is the estimation of the interactions between factors i and j .

2.8 Quantum chemistry parameter

Density functional theory (DFT) calculations were conducted using the Gaussian 16 software package to examine the geometric structures and vibrational frequencies of the molecules. The B3LYP functional and the 6-311G+(d,p) basis set were utilized for geometry optimization and frequency calculations. This choice of basis set considers dispersion interactions, which are crucial for accurate modeling of intermolecular forces [21]. The Fukui index is based on the finite difference approximation (FDA) and the NBO electron populations of the $N-1$, N , and $N+1$ electron systems to obtain the three defined functions [21]. In addition to the experimental analysis, a computational study was employed to simulate the adsorption process. The goal was to investigate how LEVO and MNZ antibiotics interact with the surface of biochar containing oxygen-containing functional groups (O-functional groups). To achieve this, biochar models were constructed that incorporated two types

of O-functional groups: hydroxyl (-OH) and a combined hydroxyl and carbonyl group (-OH-CHO). These models consisted of a structure containing 14 aromatic rings, with hydrogen atoms terminating the edges for stability.

To quantify the strength of the adsorption interactions, a parameter called adsorption energy (E_{ad}) was calculated. This value is determined using the following equation:

$$E_{ad} = E_{AB} - (E_A + E_B)$$

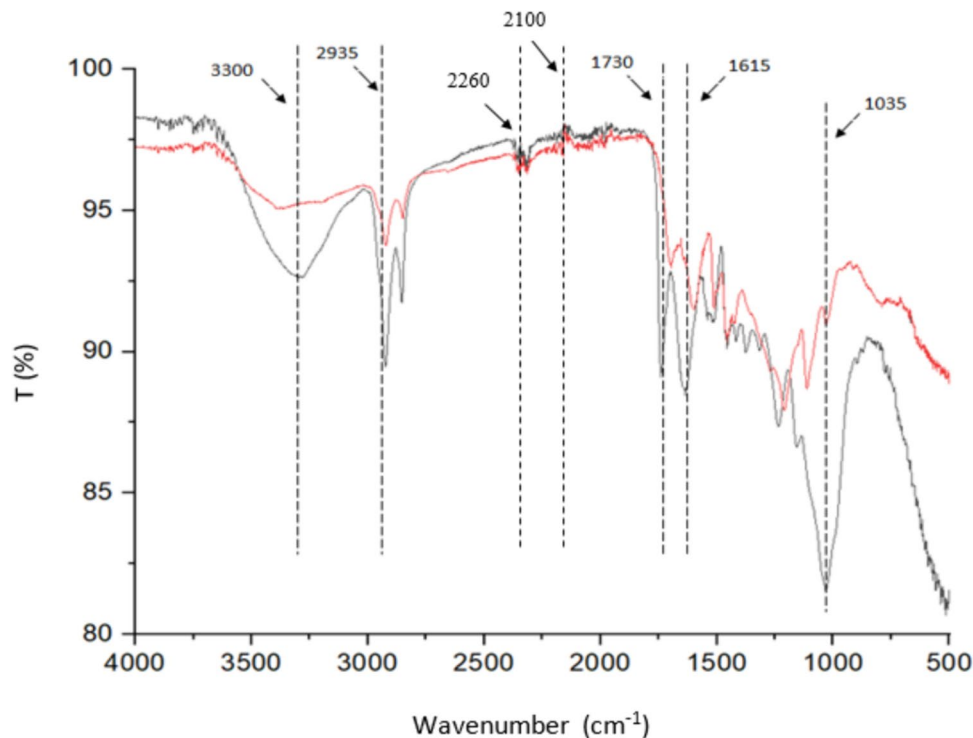
Here, E_{AB} represents the total energy of the combined system (adsorbed molecule + biochar with O-functional groups), while E_A and E_B represent the individual energies of the isolated adsorbed molecule and the biochar surface, respectively.

3 Results and discussion

3.1 Characterization of HSHC

A Fourier Transform Infrared (FTIR) analysis was performed within the spectral range of 4000–400 cm^{-1} enabled the characterization of surface functional groups present on the hydrochar from hawthorn seeds (HSHC) (Fig. 2). Comparing the FTIR spectra of hawthorn seeds (HS) and hydrochar (HSHC) revealed changes. The presence of the band at 3300 cm^{-1} , attributed to -OH groups, suggests their association with humidity or cellulose components, although

Fig. 2 FTIR spectra of HSHC and HS



these groups were reduced in hydrothermal hydrochars [22]. Moreover, the IR spectrum illustrates a decarboxylation trend from HS to HSHC, with the decrease in intensity indicating the hydroxylation process under hydrothermal conditions. Peaks at 1730 cm^{-1} indicate C=O stretching, while those around 1615 cm^{-1} signify C–O bonds [23]. The absorption peak at $2100\text{--}2260\text{ cm}^{-1}$ could be attributed to the C≡C stretching of alkyne. Furthermore, the $\nu(\text{C–H})$ stretching vibrations of aliphatic chains are apparent at 2935 cm^{-1} [24]. The band associated with C=C group stretching indicates the presence of lignin in the hydrochar [25].

The surface images of HSHC and HS were recorded to reveal the surface morphology. Figure 3 displays SEM analysis findings regarding the structure and chemical composition of the adsorbents. It was shown that hawthorn seed feedstock exhibited a tight block structure without pores, as depicted in Fig. 3 (a,b) where a series of large holes, varying in size from 30 to 200 μm , are spread across the cross-section. The surface of HS appeared relatively

smooth with fewer indentations. However, the conversion of HS to HC brought about a change in surface structure, yielding a more porous surface as shown in Fig. 3 (c,d). This transformation resulted in enhanced irregularity and the formation of cavities due to hydrothermal conditions, leading to distinct grains, pores, and channels on the surface [26]. These alterations contributed to increased specific surface areas, thereby facilitating the adsorption process.

Figure 4 displays the X-ray diffraction patterns of the carbonized HSHC material. The cellulose crystallites are small, typically around 5 nm in width, which limits the resolution of the X-ray diffraction (XRD) pattern for extracting precise information about crystal lattices within the structure. Cellulose crystallites are known to have defects, allowing XRD to identify the amorphous regions where a significant portion of the cellulose structure is less regular [27]. In Fig. 4, the broad peak at approximately 21.5° corresponds to the amorphous contribution of cellulose.

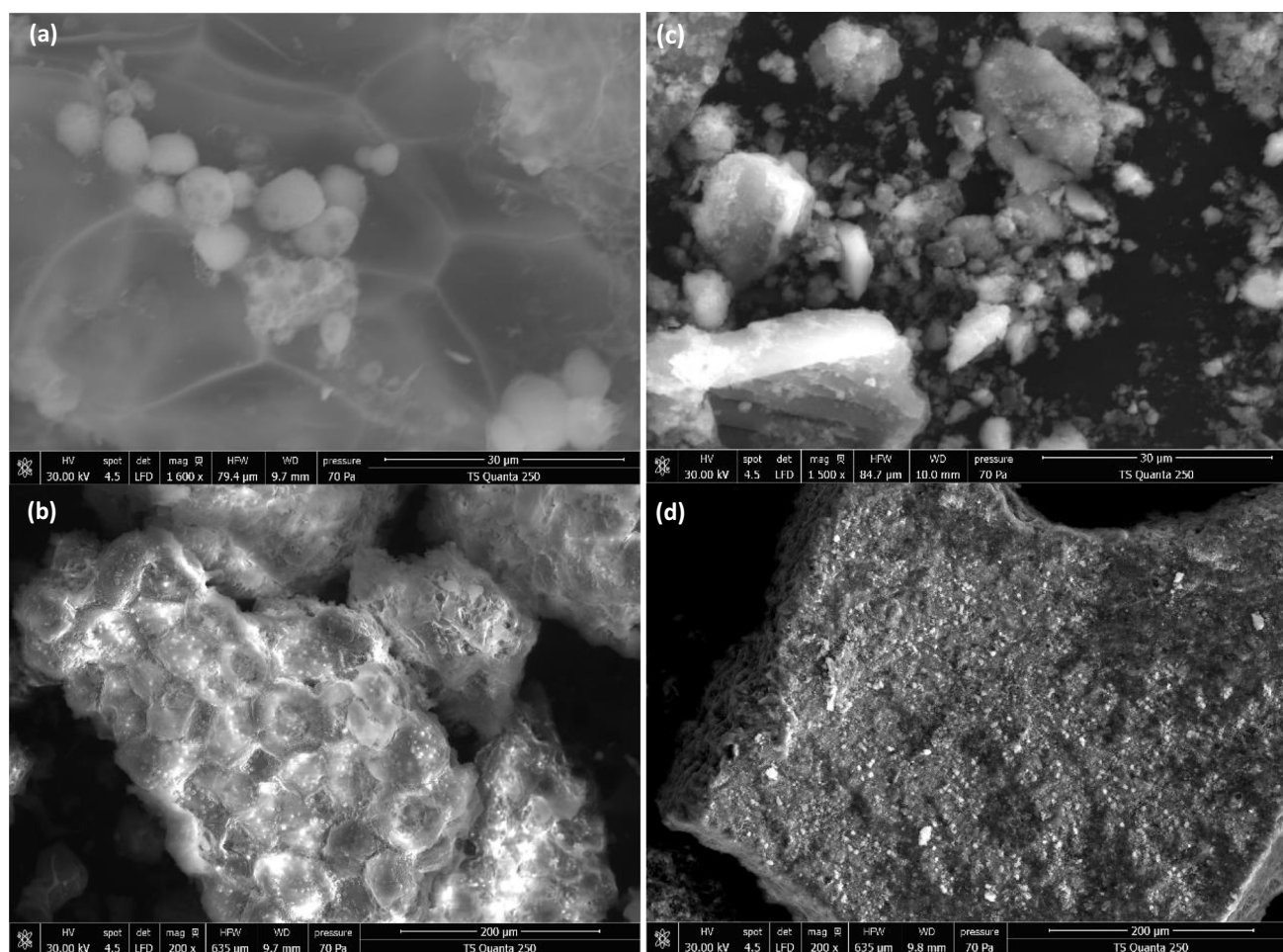


Fig. 3 SEM images of HSHC (a, c) and HS (b, d)

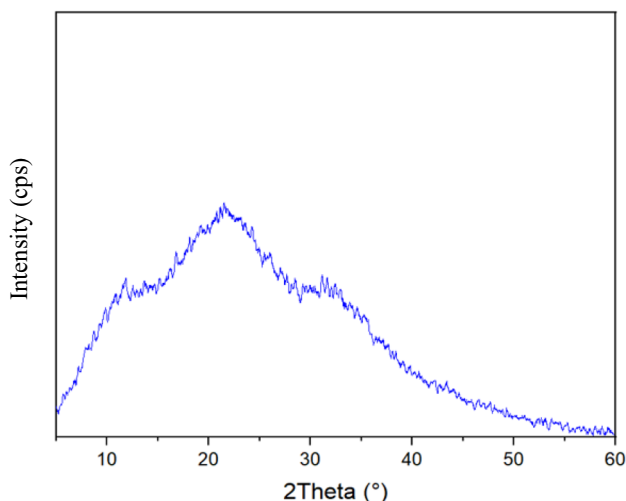


Fig. 4 XRD patterns of HSHC

3.2 Determination pH_{pzc}

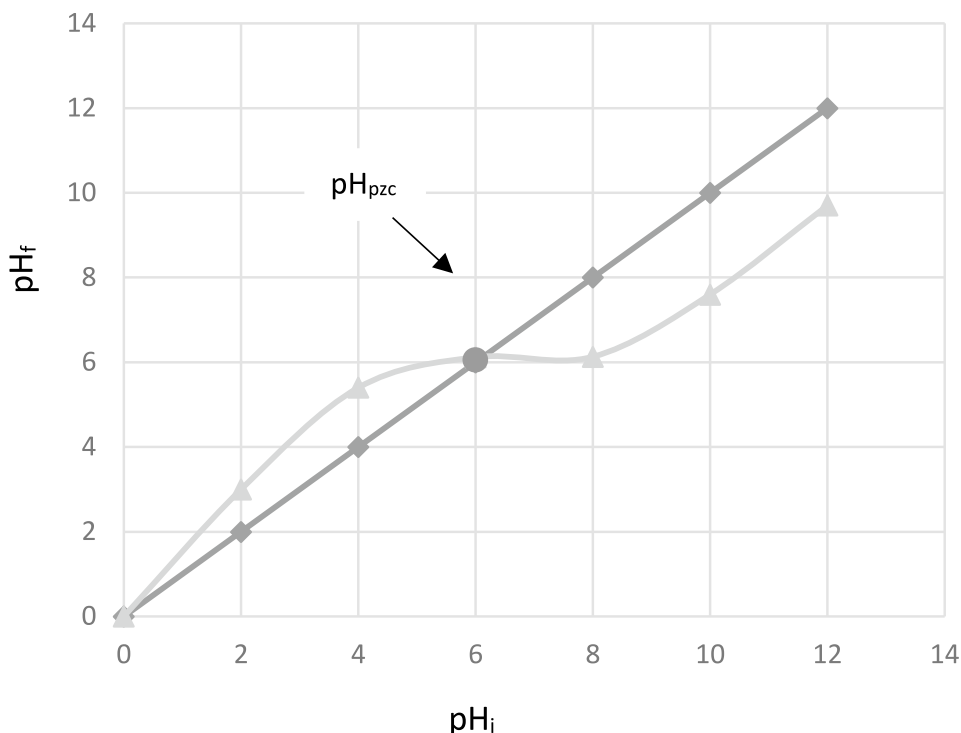
The pH of aqueous solutions plays a crucial role in the adsorption process, as it influences both the ionization of antibiotics and the surface charge of hydrochar [28]. The surface charge of HSHC was determined by examining its point of zero charge (pH_{pzc}). As shown in Fig. 5, the pH_{pzc} of HSHC was found to be 6.15. Consequently, the surface of HSHC carries a positive charge when the pH is

below 6.15 and a negative charge when the pH exceeds 6.15. When the pH is lower than the pK_a of antibiotics and the pH_{pzc} , the net surface charge of HSHC becomes positive, thereby impeding the sorption of neutral antibiotics [29]. Conversely, at a pH higher than both the pK_a and pH_{pzc} , both the HSHC surface and the antibiotics would be negatively charged, resulting in repulsion. The pK_a values for LEVO and MNZ are 6.25 and 2.57, respectively. Therefore, maintaining the solution pH around 4 is optimal to prevent an opposite charge state between ATB molecules and HSHC, facilitating electrostatic attraction and enhancing antibiotic adsorption. However, if the pH of the solution increases to 6, both ATB and HSHC will be in the same charge state, leading to electrostatic repulsion.

3.3 Adsorption kinetics and isotherm

The extraction time is critical in reaching equilibrium in kinetic studies, defining the partition of micropollutants between solid phases and aqueous solutions [29]. The effect of contact time on the adsorption of LEVO and MNZ was investigated over 70 min. As shown in Fig. 6, adsorption rates increased rapidly during the initial phase of the trials, with a quick removal rate observed within less than 5 min. This rapid adsorption can be attributed to the abundant presence of pores on the surface of the adsorbent material [30]. After the initial 5-min period, the adsorption efficiency continued to increase gradually, indicating a potential onset

Fig. 5 pH_{pzc} of HSHC



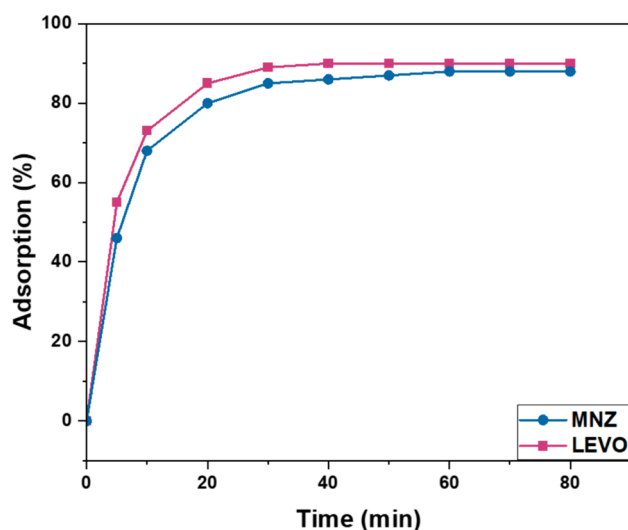


Fig. 6 The effect of contact time

of pore saturation. By the 30-min mark, the removal rate had stabilized significantly, signifying the attainment of equilibrium and saturation of sorption sites.

3.4 Kinetic and equilibrium essays

Adsorption kinetics were analyzed to explore the mechanism of LEVO adsorption. The kinetic models studied included the pseudo-first-order (PFO) and pseudo-second-order (PSO) models, with their corresponding equations provided in Table 4. The kinetic parameters obtained were summarized in the Table 2. It was evident that the pseudo-second-order (PSO) model best described the adsorption process

Table 4 Refinement of Parameter Values in Kinetic and Isotherm Models for Levofloxacin Adsorption by HSHC

Models	Parameters	Values
Pseudo-first order	Q_e (mg g^{-1})	3.180
	k_1 (min^{-1})	0.001
	R^2	0.8643
	SSE	3.987
Pseudo-second first	Q_e (mg g^{-1})	9.417
	k_2 ($\text{g mg}^{-1} \text{min}^{-1}$)	0.054
	R^2	0.998
	SSE	0.0990
Freundlich	K_F (mg g^{-1}) (mg L^{-1}) $^{-1/n}$	10.742
	n	2.531
	R^2	0.9688
Langmuir	Q_m (mg g^{-1})	63.251
	K_L	0.215
	R^2	0.9876

of LEVO, as indicated by its higher coefficient value of R^2 and smaller sum of squared errors (SSE) compared to the pseudo-first-order (PFO) model. The pseudo-second-order (PSO) model suggests that the rate-limiting step in the LEVO adsorption process could be attributed to physicochemical interactions between phases, facilitating the removal of LEVO from solution.

The Langmuir and Freundlich models were analyzed to study both heterogeneous and homogeneous surface adsorption of the adsorbent. Their respective linear equations were presented in the Table 4. The obtained correlation coefficients R^2 were 0.9876 for the Langmuir model and 0.9688 for the Freundlich model, demonstrating strong fits for both.

3.5 Optimization of SPE parameters

After confirming the adsorption of antibiotics on the synthesized hydrochar HSHC. Factors influencing the solid phase extraction procedure of antibiotics were optimized. A mixed matrix design was employed to study multiple factors and their interaction effects on the responses across all experimentally studied fields using AZURAD software. Eighteen experiments were randomly conducted according to the experimental design (Table 5). The equation relating the tested factors to the extraction recovery is as follows (9)

Table 5 Mixed experimental design and results

No. exp	Sample volume (mL)	Elution volume (mL)	Elution solvent nature	R (%)	
				LEVO	MNZ
1	50	1	MeOH	17.29	15.41
2	50	1	DCM	8.12	7.39
3	150	1	MeOH	12.65	11.59
4	150	1	ACN	9.78	9.41
5	50	5	ACN	83.39	81.22
6	50	3	DCM	27.14	26.05
7_1	100	3	ACN	65.27	65.09
7_2	100	3	ACN	66.78	65.12
7_3	100	3	ACN	65.45	64.87
8	150	1	DCM	6.74	5.89
9	100	1	DCM	7.19	6.64
10	50	1	ACN	11.31	10.70
11	150	3	DCM	23.24	21.14
12	50	5	MeOH	96.39	96.22
13	100	5	MeOH	90.59	90.03
14	50	5	DCM	48.50	47.76
15	100	5	DCM	44.12	43.84
16	150	5	MeOH	87.52	86.21
17	150	5	ACN	71.87	70.02
18	150	5	DCM	37.52	36.69

$$\begin{aligned}
 Y = & 36.18 - 2.71X_1 + 18.01X_2 + 34.65X_3 \\
 & + 25.71X_3 - 5.37X_1^2 - 10.94X_2^2 - 1.98X_1X_2 \\
 & - 0.66X_1X_{3A} - 0.55X_1X_{3B} + 18.91X_2X_{3A} \\
 & + 16.98X_2X_{3B}
 \end{aligned} \quad (9)$$

In Eq. (9), the parameter X_1 (sample volume) obtained a negative effect that this factor adjusting to the lowest level should increase the extraction recovery. The parameters X_2 (elution volume) and X_3 (solvent elution nature) resulted in a positive effect on the studied response.

The graph in Fig. 7 illustrates the relationship between extraction time and elution volume versus the nature of solvent elution. The nature of the elution solvent significantly influences the adsorption of target analytes onto the adsorbent.

Figure 8 illustrates the two-dimensional (2D) response surface plots depicting the main factors, such as sample volume, solvent elution volume, and nature of solvent elution. To maximize extraction recovery, two-dimensional (2D) response surfaces were plotted for sample volume and solvent elution volume, with the nature of solvent elution held constant for LEVO and MNZ.

Based on our previous work [7, 31], acetonitrile, methanol, and dichloromethane, being the most frequently utilized elution solvents, were chosen for this investigation. These solvents have been extensively utilized in numerous studies for the extraction of antibiotics (ATB). The extraction recovery is closely linked to the choice of elution solvent. Methanol was selected as the elution solvent due to its ability to achieve maximum elution. The eluent volume greatly influences the recovery of antibiotics from HSHC-packed cartridges. As the volume increases, extraction efficiency improves, as expected. However, when applying a water sample to the cartridge, analytes are loaded onto the HSHC until the breakthrough volume is reached. Breakthrough occurs when the adsorbent's capacity is reached. Beyond the breakthrough volume, analytes are eluted along with the sample matrix.

It was indicated that the extraction efficiency is highest when the elution volume is around 4.5–5 mL and 70–75 mL of sample volume with methanol, as shown in Fig. 8a, compared to ACN and DCM in Figs. 8b and c. Methanol was identified as the optimal solvent due to its strong affinity for the analytes.

Model validation can also be performed graphically by comparing calculated and experimental ATB extraction recovery values. This relationship is illustrated in Fig. 7 a and b, indicating a close alignment between calculated and experimental extraction recovery values, thereby confirming the statistical validation of the model. Based on Fig. 7, the mixed matrix model was excluded from the second-order polynomial model.

3.6 Validation of the optimized method

The optimized SPE-HSHC-HPLC/UV method validation parameters focused on linearity and sensitivity. Linearity of studies products was assessed at five concentration levels ranging from 0.31 $\mu\text{g/mL}$ to 5 $\mu\text{g/mL}$ for LEVO and MNZ. All antibiotics studied exhibited excellent linearity, with r^2 values coefficient of 0.996 and 0.997, respectively. The method validation included assessing the limit of detection (LOD) and limit of quantification (LOQ) under optimal conditions. Table 6 summarizes the LOD values, determined using the signal-to-noise ratio ($3 \times S/N$), which were 0.13 $\mu\text{g/mL}$ for LEVO and 0.2 $\mu\text{g/mL}$ for MNZ. The LOQ values, determined using a signal-to-noise ratio of $10 \times S/N$, were 0.62 $\mu\text{g/mL}$ for LEVO and 0.87 $\mu\text{g/mL}$ for MNZ.

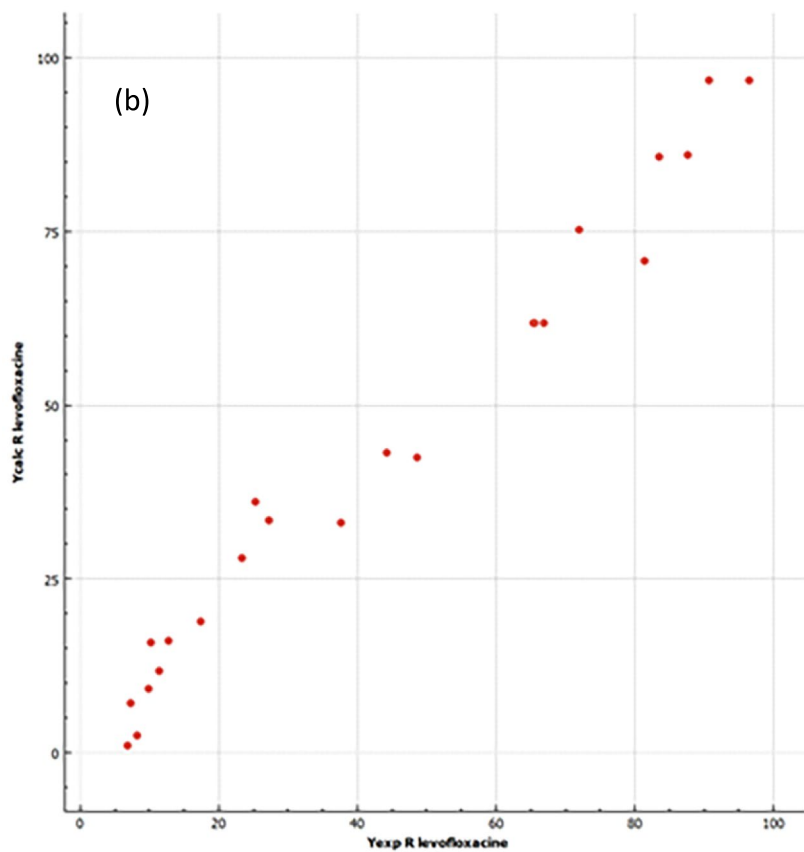
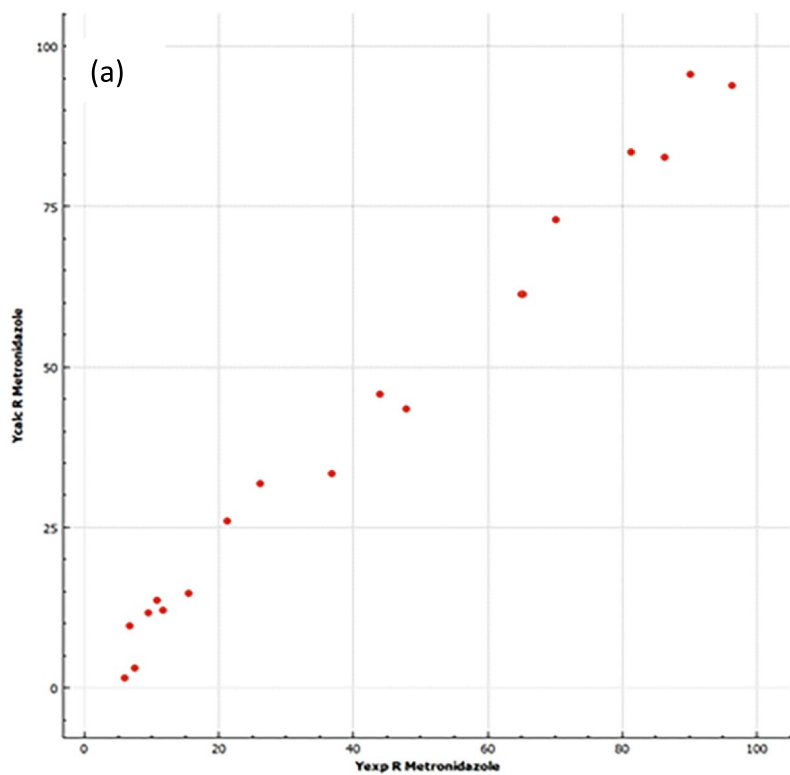
3.7 Comparative study

A comparative analysis between the developed solid phase extraction method and other relevant solid phase procedures from the literature was conducted to analyze LEVO and MNZ in water samples using liquid chromatography. Table 7 illustrates the effectiveness of the proposed method for antibiotic analysis in water samples.

3.8 Regeneration and application

Regeneration is a crucial characteristic of adsorbents. The reusability of the HSHC was evaluated through multiple rounds of SPE experiments, extending up to five cycles. The material was thoroughly cleansed using a combination of methanol and water before being reintroduced into the SPE process. However, the extraction efficiency of HSHC for antibiotics showed a slight decline with each regeneration of the adsorbent, as depicted in Fig. 9. By the fifth cycle, the extraction recovery had dropped to 80%, suggesting that while the prepared HSHC demonstrated reasonable reusability during the solid-phase extraction (SPE) process, its efficiency decreased after successive cycles. To assess the applicability of HSHC in environmental sample analysis. All optimized solid-phase extraction (SPE) conditions were assessed using real water samples contaminated from various sources: tap water from our laboratory with a pH of 7, effluent from the wastewater treatment plant (WWTP) at El HESSIANE in northern Greater TUNIS with a pH of 6.5, and wastewater from the pharmaceutical industry (SAIPH) located on the Road to ZAGHOUAN with a pH of 7.5. The HSHC has shown its capability in extracting two antibiotics from samples of surface water. Recovery studies were conducted using water samples spiked with 1 $\mu\text{g/L}$ of each drug. The results are shown in Table 8, where average recoveries exceeded 90%, and the relative standard deviation (RSD) ranged from 3 to 9%.

Fig. 7 Plots of the relationship between the predicted and actual values of extraction recoveries (%): **(a)** MNZ and **(b)** LEVO



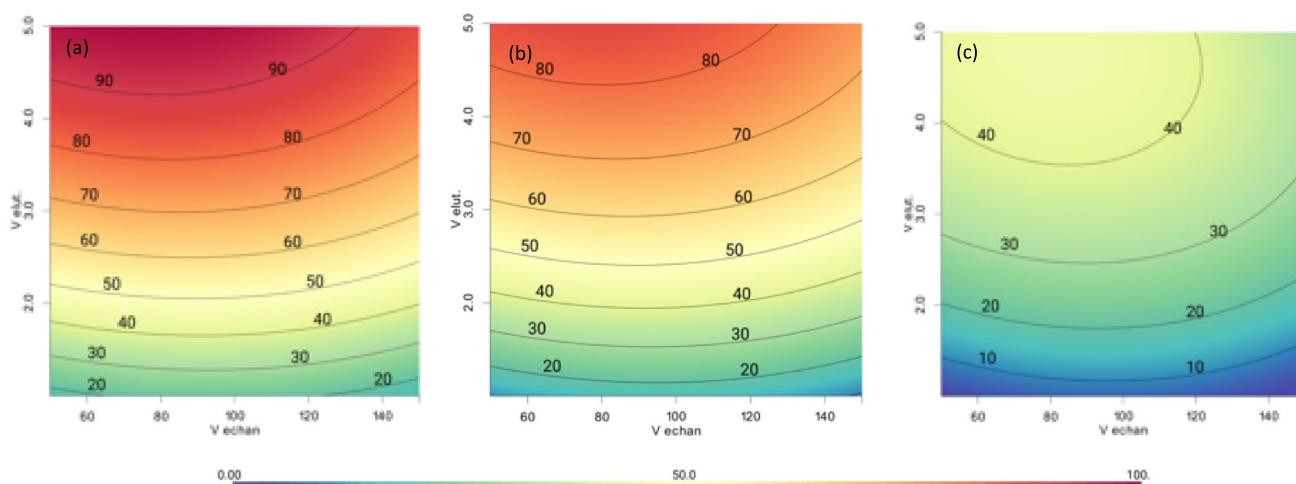


Fig. 8 Surface plot (cutting plane) at fixed variables: sample volume (mL), solvent elution volume (mL), and nature of solvent elution

Table 6 Correlation coefficients, Recovery percentage, LOD, and LOQ obtained from the application of SPE-HSHC-HPLC/UV method in a water sample

Antibiotics	Linearity	Recovery	Sensitivity	
	R ²	R%	LOD ($\mu\text{g.L}^{-1}$)	LOQ ($\mu\text{g.L}^{-1}$)
Levofloxacin	0.996	96.39	0.13	0.62
Metronidazol	0.997	96.22	0.2	0.87

3.9 Quantum chemistry simulation results

To further explore the possible adsorption mechanism, The HOMO and LUMO orbital contributions for the studied molecules were calculated using the B3LYP/6–311 + G(d,p) level of theory. The highest occupied molecular orbital (HOMO) and lowest unoccupied molecular orbital (LUMO) of LEVO and MNZ indicate their ability to lose or gain electrons [36]. According to Fig. 10(b), the HOMO orbital of LEVO is primarily located at the pyridine ring, benzene binding, and the heteroatom F, making these sites susceptible to attack by electrophilic sites of biochar. Conversely, the LUMO orbital

of LEVO, as shown in Fig. 10(c), is predominantly situated at the pyridine ring, benzene binding, and carboxylic acid, indicating susceptibility to attack by nucleophilic active sites of the adsorbent. Furthermore, the HOMO of MNZ is primarily located at the nitro group and the piperazine ring. Similarly, the LUMO is entirely situated at the piperazine ring.

Additionally, as depicted in Fig. 10(d), electrostatic potential (ESP) mapping on the surfaces of LEVO and MNZ molecules shows that regions surrounding the pyridine ring, benzene binding, and carboxylic acid are likely to be susceptible to attack by negatively charged OH groups, thereby promoting interfacial reactions. This finding aligns with O-containing groups and nitrogen being the primary reactive species in the adsorption of LEVO and MNZ.

Regarding the Fukui index representing the electrophilic (f^-) and nucleophilic (f^+) values of LEVO and MNZ molecules, as listed in Table 1, higher f^- values suggest susceptibility to attack by electrophilic sites, while higher f^+ values indicate susceptibility to attack by nucleophilic sites. For the LEVO molecule, active sites such as C3, F12, N13, O16, O17, O20, C22, N30, N33, C34 are more likely to be attacked by electrophilic radicals, while sites like C2, H6,

Table 7 Reported solid phase extraction methods for the determination of ATB in water samples

Micropollutants	Analytical method	Sorbent	Recovery (%)	Q(mg/g)	Ref
Metronidazole	UV–Vis	three-dimensional ordered carbon foam derived from liquefied eucalyptus sawdust	84.6	42.92	[32]
Metronidazole	UV–Vis	self-shaping porousbiomasscarbonfoampellets	93.9	64.23	[33]
levofloxacin	HPLC/PDA	nano-zero-valent iron and nano-copper	92	0.127	[34]
levofloxacin	HPLC–UV	Carboxylated cellulose nanofiber/montmorillonite nanocomposite	93.97	65.901	[35]
Levofloxacin Metronidazole	HPLC–UV	Hawthorn seeds hydrochar	96	63.251	The present work

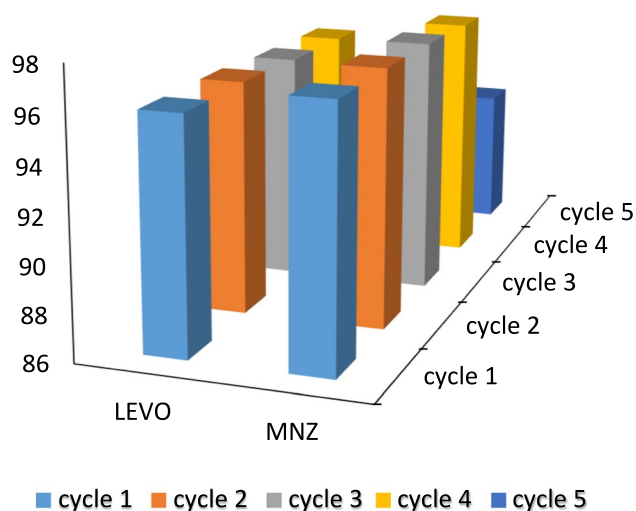


Fig. 9 ATB removal efficiencies in five successive recycleruns

Table 8 Recovery percentages and relative standard deviations (RSDs) obtained from the extraction of antibiotics in water samples

Antibiotics	Recovery % (CV)		
	Tap water	WWTP water	(SAIPH)
Levofloxacin	92.74 (5.23)	91.58 (8.51)	94.85 (8.89)
Metronidazol	91.12 (4.02)	90.66 (7.64)	95.31(7.40)

C8, C11, C15, H18, H23, H27, H39 are more susceptible to nucleophilic radicals.

In contrast, for the MNZ molecule, sites such as N7 are more likely to be attacked by electrophilic radicals, while sites like C2, C10, and C18 are more susceptible to nucleophilic radicals. (Table 9).

In Fig. 11. as per the simulation process, the studied contaminants exhibit maximum adsorption energies represented by negative values. The results indicate that the adsorption energies (Eads) of LEVO on the surface are -64.12 kJ/mol for C-OH-CHO, 54.78 kJ/mol for C-OH, and 50.17 kJ/mol for C biochar. In contrast, the adsorption energy of MNZ on the biochar surface is lower compared to that of LEVO.

From Fig. 11. the dotted line between the contaminant and the biochar surface indicates a strong van der Waals interaction. Additionally, the presence of an unoccupied overlapping area at the center of each benzene ring signifies the steric effects within the molecules [37]. The surface area of the contaminant adsorbed on the biochar model with OH-CHO is the largest, indicating a wider van der Waals interaction area, corresponding to maximum adsorption energies of -64.12 kJ/mol for LEVO and -59.37 kJ/mol for MNZ. This suggests that biochar with O-functional groups adsorbs LEVO and MNZ, where the oxygen-containing functional groups form weak hydrogen bonds with the phenolic

hydroxyl group and nitrogen of contaminants. These interactions are crucial for enhancing the adsorption capacity of contaminants by hydroxyl and other oxygen-containing functional groups [38].

For calculating the molecular adsorption distance, it's important to note that the planes of the two molecules are not parallel, and even the atoms within a single molecule are not all on the same plane. The calculated distance is the distance between the center point of the benzene ring on the contaminant and the projected point on the biochar. The promoting effect of O-containing functional groups on the adsorption of LEVO and MNZ primarily involves the electron pair donation from the ortho-position carbon atom, enhancing the electrostatic effect. Additionally, the O and H atoms on LEVO and MNZ form weak hydrogen bonds with the H and O atoms on biochar, respectively. Another significant mechanism in the adsorption of nitrogen and benzene rings with carbon-based materials is π - π interaction, where the π orbital on the carbon-based plane interacts with the π electron cloud on the benzene ring.

Comparing the adsorption results in Fig. 11(a), (b), and (c) confirms that hydroxyl groups enhance adsorption. This is mainly because hydroxyl groups, as electron-donating groups, strengthen the interaction between electron clouds, thereby reinforcing π - π interactions [12].

4 Conclusion

A novel method using SPE-HPLC/UV for simultaneous quantification of antibiotics Levofloxacin and Metronidazole has been developed. New hydrochar of hawthorn seeds has been successfully prepared using a hydrothermal method to remove ATB contaminations. The HSHC was characterized using Fourier-transform infrared (FTIR) spectroscopy and scanning electron microscopy (SEM). Then levofloxacin was chosen to examine the sorption of antibiotics on HSHC. Equilibrium adsorption is achieved within 30 min, reaching a maximum recovery adsorption capacity of 96% at pH 4.0 and 25°C. The mixed matrix experimental design used to optimize variables for extracting antibiotics (ATB) with synthesized HSHC showed significant effects of sample volume, solvent elution volume, and solvent nature, along with their interactions. The optimal conditions involved a sample volume of 75.5 mL and a solvent elution volume of 5 mL, with methanol being used as the elution solvent. The extraction recovery for all antibiotics exceeded 96.3%, with detection limits ranging from 0.13 to 0.2 μ g/L. These results highlight the potential of HSHC as a new biosorbent in solid-phase extraction devices for efficiently removing antibiotics from surface water, offering short analysis times, minimal waste generation, and cost-effective material preparation. According to DFT calculations, the Fukui function identifies nucleophilic and electrophilic attack sites in antibiotics. In conclusion, O-containing functional groups enhance the adsorption

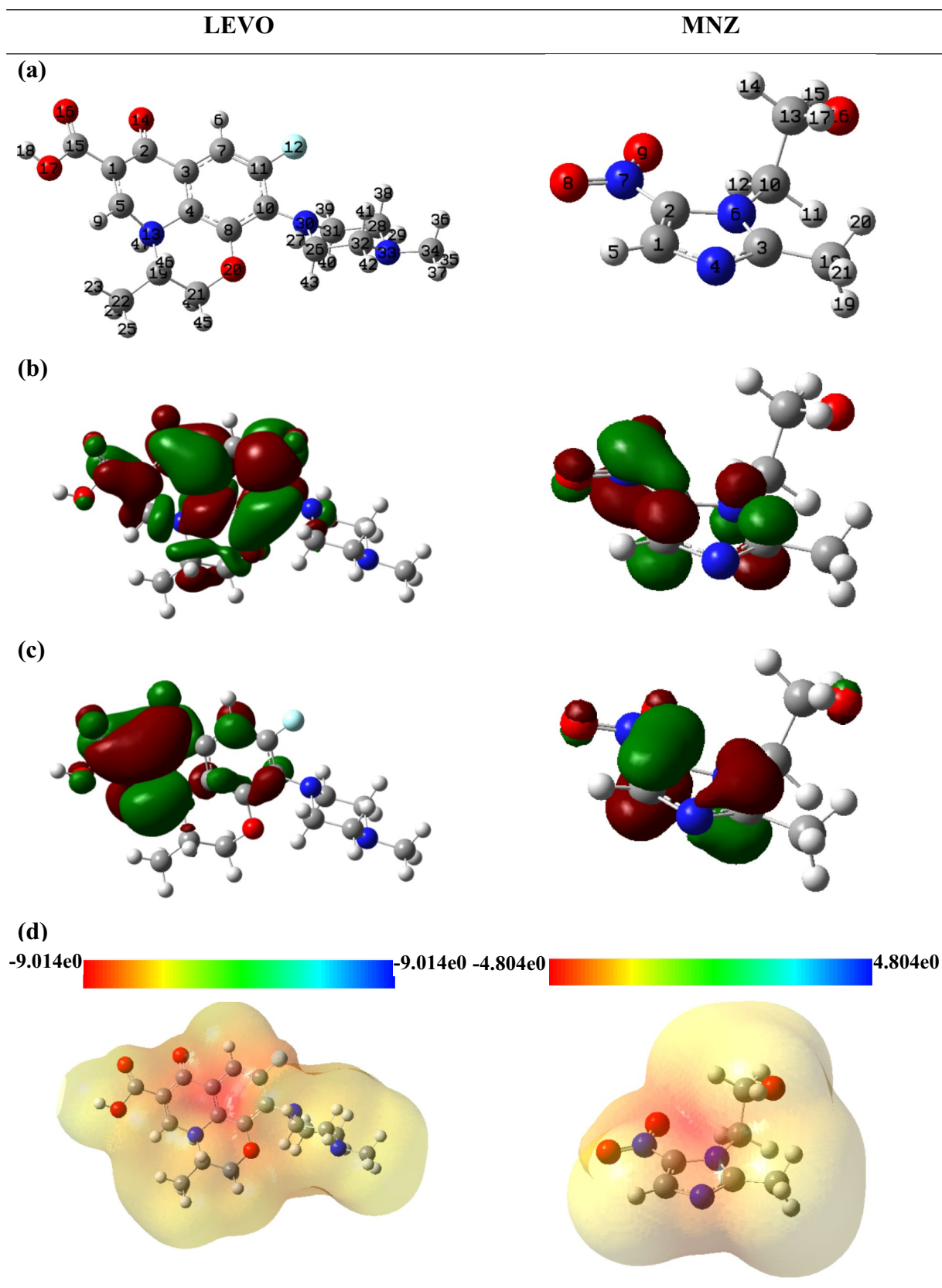


Fig. 10 Computed quantum parameters of LEVO and MNZ calculated using the Gaussian 16 program at the B3LYP/6-311G+(d,p) level: (a) Geometric optimization (b) Isodensity surfaces of the HOMO, (c) LUMO and (d) Electrostatic potential (ESP) mapping

Table 9 Fukui index (f^- and f^+) for electrophilic and nucleophilic attacks of the molecule with N electrons and $q(N+1)$, $q(N-1)$ calculated at the B3LYP/6-311G+(d,p) level of theory

Levo				MNZ			
N°	Atom	f^-	f^+	N°	Atom	f^-	f^+
1	C	-0.0570	-0.1169	1	C	-0.1175	-0.1425
2	C	-0.2791	0.1989	2	C	-0.1949	0.0165
3	C	0.1002	-0.0729	3	C	-0.1747	-0.0945
4	C	-0.0589	0.0617	4	N	-0.0559	-0.0351
5	C	-0.4061	0.0345	5	H	-0.0374	-0.0255
6	H	-0.1366	0.1131	6	N	-0.0340	-0.0253
7	C	0.0633	-0.1196	7	N	0.0422	-0.1273
8	C	-0.1333	0.1267	8	O	-0.1117	-0.2120
9	H	-0.1286	0.0730	9	O	-0.0891	-0.2148
10	C	-0.1069	0.0206	10	C	-0.0080	0.0279
11	C	-0.2039	0.1694	11	H	-0.0172	-0.0308
12	F	0.1629	-0.2053	12	H	-0.0090	-0.0178
13	N	0.2439	-0.2447	13	C	0.0067	-0.0007
14	O	0.0692	-0.3216	14	H	-0.0134	0.0082
15	C	-0.3850	0.3831	15	H	-0.0277	-0.0442
16	O	0.1653	-0.3153	16	O	-0.0486	-0.0153
17	O	0.3257	-0.3615	17	H	-0.0076	0.0019
18	H	-0.2625	0.2156	18	C	0.0086	0.0392
19	C	0.0058	-0.0273	19	H	-0.0443	-0.0456
20	O	0.2494	-0.2832	20	H	-0.0383	-0.0365
21	C	0.0182	-0.0097	21	H	-0.0283	-0.0259
22	C	0.3004	-0.2916				
23	H	-0.1090	0.1073				
24	H	-0.1125	0.0950				
25	H	-0.1351	0.0859				
26	C	0.0855	-0.0673				
27	H	-0.0992	0.1036				
28	C	0.0875	-0.0846				
29	H	-0.1105	0.0877				
30	N	0.1937	-0.2873				
31	C	0.0819	-0.0646				
32	C	0.0832	-0.0821				
33	N	0.2762	-0.2793				
34	C	0.1759	-0.1684				
35	H	-0.1040	0.0898				
36	H	-0.0845	0.0730				
37	H	-0.1022	0.0897				
38	H	-0.0861	0.0796				
39	H	-0.1098	0.1096				
40	H	-0.0950	0.0674				
41	H	-0.0827	0.0726				
42	H	-0.1085	0.0860				
43	H	-0.0989	0.0784				
44	H	-0.0943	0.0655				
45	H	-0.1219	0.0746				
46	H	-0.1055	0.0795				
47	H	-0.2720	0.0586				

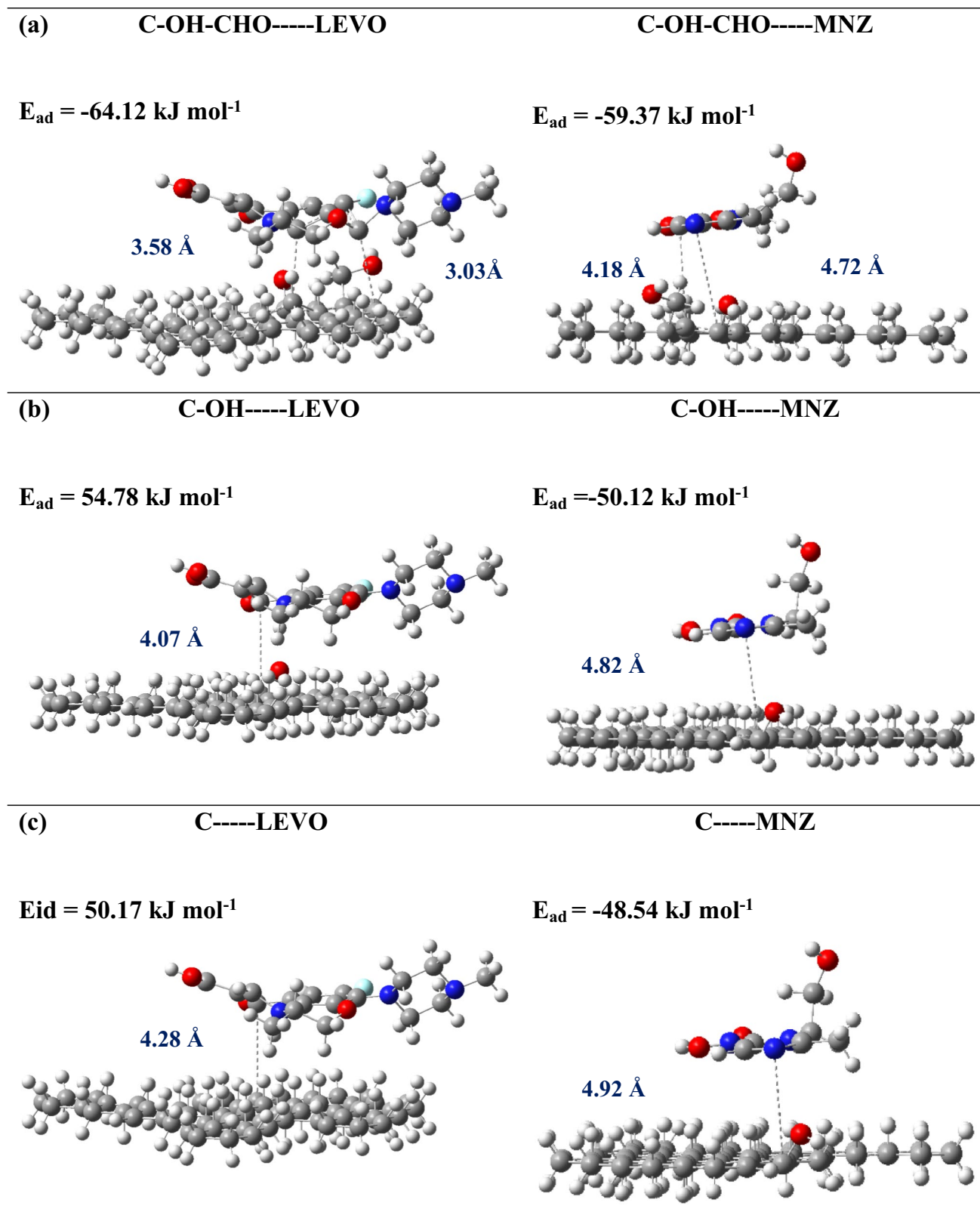


Fig. 11 LEVO and MNZ adsorption by biochar (a) C-OH-CHO—LEVO and C-OH-CHO—MNZ; (b) C-OH—LEVO and C-OH—MNZ; (c) C—LEVO and C—MNZ

of LEVO and MNZ by altering the electrostatic potential on biochar surfaces, shifting contaminant adsorption sites, and increasing van der Waals interactions between molecules.

Author contributions A. SNOUSSI: Formal Analysis, Conceptualization, Writing Original Draft, I. ABIDL: Formal Analysis, Writing Original Draft, R. Bensghaier: Editing including analysis of data. M. CLAEYS: Analysis of data, L. LATROUS: overall supervision of the work, Methodology, Writing, Review, A. MEGRICHE: Review. All authors have read and agreed to the published version of the manuscript.

Funding Not applicable.

Data availability Data will be made available on request.

Declarations

Ethical approval Not applicable.

Informed consent Not applicable.

Conflict of interest The authors have no conflict of interest in preparation of this manuscript.

References

1. FAO (Food and Agriculture Organization of the United Nations). *Leveraging Food Systems for Inclusive Rural Transformation*. Rome: Food and Agriculture Organization of the United Nations, 2017
2. M.A. Abdallah, R.B. Sghaier, M. Zougagh, L. Latrous, A. Megriche, *Anal. Methods* **16**, 1870–1879 (2024)
3. S. Jadoun, R. Arif, N.K. Jangid, R.K. Meena, *Environ. Chem. Lett.* **19**, 355–374 (2021)
4. S.M. Shaheen, A. Natasha, A. Mosa, M.F. El-Naggar, H. Hossain, N.K. Abdelrahman, M. Niazi, T. Shahid, Y.F. Zhang, L. Tsang, S. Trakal, J.R. Wang, *Bioresour. Technol.* **346**, 126581 (2022)
5. R.N. de Sousa, M.B. Soares, F.H. dos Santos, C.N. Leite, K.F. Mendes, in *Interactions of Biochar and Herbicides in the Environment* (CRC Press, 2022)
6. C.Y. Teo, J.S.J. Jong, Y.Q. Chan, W. Oueslati. Carbon-Based materials as effective adsorbents for the removal of pharmaceutical compounds from aqueous solution. *Adsorp. Sci. Technol.* **2022**, (2022). <https://doi.org/10.1155/2022/3079663>
7. R. Bensghaier, I. Thili, L. Latrous, A. Megriche, *Chem. Afr.* (2022). <https://doi.org/10.1007/s42250-022-00405-5>
8. R. Bensghaier, A. Snoussi, M. Aouled Abdallah, L. Latrous, A. Megriche, *New J. Chem.* (2023). 10.1039/D2NJ05568F
9. L. Latrous, Optimization and validation in liquid chromatography using design of experiments. *Chem Afr* **5**, 437–458 (2022). <https://doi.org/10.1007/s42250-022-00344-1>
10. A.M. Khalil, E.D. Van Hullebusch, M.M. Chehimi, *Chem. Afr.* **6**, 559–560 (2023)
11. I.A. Aguayo-Villarreal, D. Cortes-Arriagada, C.K. Rojas-Mayorga, K. Pineda-Urbina, R. Muñoz-Valencia, J. González, *J. Mol. Struct.* **1203**, 127398 (2020)
12. S. Yu, X. Wang, Y. Ai, X. Tan, T. Hayat, W. Hu, X. Wang, *J. Mater. Chem. A* **4**, 5654–5662 (2016)
13. A. K. Chandra, M. T. Nguyen. in *Chemical Reactivity Theory: A Density-Functional View*, ed. by P. K. Chattaraj (Taylor and Francis, New York, 2008), p. 163
14. L. Sellaoui, D. Franco, H. Ghalla, J. Georgin, M. S. Netto, G. Luiz Dotto, A. Bonilla-Petriciolet, H. Belmabrouk, A. Bajahzar, *Chem. Eng. J.* **394**, 125011 (2020)
15. C. Zhang, Y. Chen, S. Chen, X. Guan, Y. Zhong, Q. Yang, *Ecotoxicol. Environ. Saf.* **255**, 114817 (2023)
16. D.O. Oyeniran, T.O. Sogbanmu, T.A. Adesalu, *Ecotoxicol. Environ. Saf.* **212**, 111982 (2021)
17. L.-T. Qin, X.-R. Pang, H.-H. Zeng, Y.-P. Liang, L.-Y. Mo, D.-Q. Wang, J.-F. Dai, *Sci. Total. Environ.* **708**, 134552 (2020)
18. M. Abd Rahim, W.A. Wan Ibrahim, Z. Ramli, M.M. Sanagi, H.Y. Aboul-Enein, *Chromatographia* **79**, 421–429 (2016)
19. L. Latrous El Atrache, R. Ben Sghaier, B. Bejaoui Kefi, V. Haldys, M. Dachraoui, J. Tortajada, *Talanta* **117**, 392–398 (2013)
20. I. Thili, R. Bensghaier, L. Latrous El Atrache, A. Megriche, *Chem. Pap.* **76**, 6941–6951 (2022)
21. I. Abidli, K. Essalah, N. Souissi, *J. Tunis. Chem. Soc.* **19**, 375–380 (2017)
22. J. Petrović, N. Perišić, J.D. Maksimović, V. Maksimović, M. Kragović, M. Stojanović, M. Laušević, M. Mihajlović, *J. Anal. Appl. Pyrolysis* **118**, 267–277 (2016)
23. Chemometric analysis of integrated FTIR and Raman spectra obtained by non-invasive exfoliative cytology for the screening of oral cancer - *Analyst* (RSC Publishing), <https://pubs.rsc.org/en/content/articlelanding/2018/an/c8an02092b/unauth>. Accessed May 7, 2024
24. P. Sanchora, D.K. Pandey, H.L. Kagdada, A. Materny, D.K. Singh, *Phys. Chem. Chem. Phys.* **22**, 17687–17704 (2020)
25. W. Sun, L. Bai, M. Chi, X. Xu, Z. Chen, K. Yu, *Energies* **16**, 1089 (2023)
26. D. Liang, Y. Liu, R. Zhang, Q. Xie, L. Zhang, A review on the influence factors in the synthesis of zeolites and the transformation behavior of silicon and aluminum during the process. *Comments. Inorg. Chem.* 1–37 (2024). <https://doi.org/10.1080/02603594.2024.2309878>
27. H. Özkaraaslan, S. Çetintaş, D. Bingöl, *Biomass. Convers. Biorefinery* **13**, 3765–3784 (2023)
28. X. Zhang, Y. Zhang, H.H. Ngo, W. Guo, H. Wen, D. Zhang, C. Li, L. Qi, *Sci. Total. Environ.* **716**, 137015 (2020)
29. J. Georgin, D.S.P. Franco, L. Meili, Y. Dehmani, G.S. dos Reis, E.C. Lima, *J. Water. Process. Eng.* **56**, 104407 (2023)
30. N. Khedri, Z. Ramezani, N. Rahbar, *Int. J. Environ. Sci. Technol.* **13**, 2475–2484 (2016)
31. R. Ben Sghaier, I. Thili, L. Latrous El Atrache, S. Net, I. Ghorbel-Abid, B. Ouddane, D. Ben Hassan-Chehimi, M. Trabelsi-Ayadi, *Int. J. Environ. Res.* **11**, 613–624 (2017)
32. Z. Hua, S. Wan, L. Sun, Z. Yu, X. Bai, *J. Chem. Technol. Biotechnol.* **93**, 3044–3055 (2018)
33. L. Sun, S. Wan, D. Yuan, Z. Yu, *Sci. Total. Environ.* **664**, 24–36 (2019)
34. M.T.M.H. Hamad, M.E. El-Sesy, *Bioresour. Bioprocess.* **10**, 1 (2023)
35. J. Li, J. Tao, C. Ma, J. Yang, T. Gu, J. Liu, *RSC Adv.* **10**, 42038–42053 (2020)
36. I. Abidli, N. Souissi, K. Essalah, X. R. Novoa, A combined experimental and theoretical approach effect of Curcuma. L extract as a corrosion inhibitor on iron in acidic solution. *Can. Metall. Q.* **63**(3), 793–811 (2023). <https://doi.org/10.1080/00084433.2023.2240113>
37. H. Xu, W. Chu, X. Huang, W. Sun, C. Jiang, Z. Liu, *Appl. Surf. Sci.* **375**, 196–206 (2016)
38. R.W. Coughlin, F.S. Ezra, *Environ. Sci. Technol.* **2**, 291–297 (1968)

Springer Nature or its licensor (e.g. a society or other partner) holds exclusive rights to this article under a publishing agreement with the author(s) or other rightsholder(s); author self-archiving of the accepted manuscript version of this article is solely governed by the terms of such publishing agreement and applicable law.